Height-resolved ionospheric drifts at low latitudes from simultaneous OI 777.4 nm and OI 630.0 nm imaging observations

J. R. Abalde, P. R. Fagundes, Y. Sahai, and V. G. Pillat
Universidade do Vale do Paraíba (UNIVAP), São José dos Campos, São Paulo, Brazil

A. A. Pimenta and J. A. Bittencourt
Instituto Nacional de Pesquisas Espaciais (INPE), São José dos Campos, São Paulo, Brazil

Received 27 April 2004; revised 4 August 2004; accepted 24 August 2004; published 16 November 2004.

[1] Transequatorial *F* region plasma bubbles are large-scale ionospheric depleted regions that develop in the bottomside of equatorial *F* region due to plasma instability processes. Simultaneous all-sky imaging observations of the OI 630.0 nm and OI 777.4 nm nightglow emissions were carried out at São José dos Campos (23.21°S, 45.86°W; dip latitude 17.6°S), Brazil, during the years 2000 and 2001, a period of high solar activity. In this work we present and discuss the height-resolved nocturnal *F* region zonal drift velocities obtained from plasma bubbles observed in imaging observations of these two emissions for several days of 2000 and 2001. It should be pointed out that the two emissions result from different excitation mechanisms (OI 630.0 nm by dissociative recombination of O_2^+ and OI 777.4 nm by radiative recombination of O^+) and come from different *F* region heights, separated by ~50–80 km. We have investigated the nighttime zonal plasma drift variations using fixed emission peak altitudes, used by earlier investigators, as well as emission peak altitudes based on simultaneous ionospheric sounding observations. The average maximum and minimum zonal plasma drift velocities inferred for both the emissions, using emission peak altitudes based on simultaneous ionospheric observations, (OI 630.0 nm: 172 ± 2 and 89 ± 15 m/s; OI 777.4 nm: 184 ± 12 and 103 ± 16 m/s) are lower and with less scatter than those using fixed emission peak altitudes (OI 630.0 nm: 185 ± 10 and 104 ± 18 m/s; OI 777.4 nm: 202 ± 19 and 121 ± 20 m/s). Also, the nocturnal variations of the zonal plasma drift velocities obtained for the two emissions with peak altitudes based on simultaneous ionospheric observations show better agreement than for the case with fixed emission peak altitudes (h = 380 km for OI 777.4 nm and h = 300 km for OI 630.0 nm). *INDEX TERMS:* 2415 Ionosphere: Equatorial ionosphere; 2437 Ionosphere: Ionospheric dynamics; 2439 Ionosphere: Ionospheric irregularities; 2494 Ionosphere: Instruments and techniques; *KEYWORDS:* ionospheric plasma drifts, ionospheric plasma bubbles, OI 777.4 nm and OI 630.0 nm emissions

Citation: Abalde, J. R., P. R. Fagundes, Y. Sahai, V. G. Pillat, A. A. Pimenta, and J. A. Bittencourt (2004), Height-resolved ionospheric drifts at low latitudes from simultaneous OI 777.4 nm and OI 630.0 nm imaging observations, *J. Geophys. Res.*, *109*, A11308, doi:10.1029/2004JA010560.

1. Introduction

[2] The ionospheric plasma density profile or electron density at any specific location, altitude, and local time are usually slightly different on consecutive days. This day-to-day variability (weather) has significant impact on the observed *F* region ionospheric parameters, such as *F* region peak heights and critical frequencies. The propagation of waves, electric fields, and neutral plasma coupling are the main sources for the ionosphere-thermosphere variability. In recent years there has been a growing interest in investigations related to the low-latitude ionospheric zonal plasma drift velocities. Zonal plasma drifts are important for a good understanding of both plasma and neutral dynamics. It is expected that the day-to-day changes in the ionosphere will influence the plasma drift velocities, which is the subject of this paper. Measurements of the zonal plasma drifts at equatorial and low-latitude regions have been carried out by several investigators using observations by satellite [e.g., *Aggson et al.*, 1987; *Coley and Heelis*, 1989; *Immel et al.*, 2003], radio technique (backscatter radar and scintillations) [e.g., *Woodman*, 1972; *Fejer et al.*, 1985; *Abdu et al.*, 1987; *Biondi et al.*, 1988; *Bhattacharyya et al.*, 1989; *Basu et al.*, 1991, 1996; *Valladares et al.*, 2002; *Kil et al.*, 2000; *de Paula et al.*, 2002], optical technique (OI 630.0 nm scanning photometer and wide-angle imaging system) [e.g., *Mendillo and Baumgardner*, 1982; *Malcolm et al.*, 1984; *Sobral and Abdu*, 1991; *Fagundes et al.*, 1997; *Taylor et al.*, 1997; *Sobral et al.*, 1999; *Pimenta et al.*, 2001; *Santana et*

0148-0227/04/2004JA010560$09.00

al., 2001; *Otsuka et al.*, 2002; *Pimenta et al.*, 2003], and multispectral optical technique (simultaneous OI 630.0 nm and OI 777.4 nm wide-angle imaging system) [e.g., *Tinsley et al.*, 1997; *Mendillo et al.*, 1997]. The ground-based wide-angle imaging system, used to infer zonal plasma drifts, is gaining importance because depending on the location, it is possible to observe the formation and evolution of large-scale ionospheric irregularities and follow their spatial and temporal variations.

[3] The OI 630.0 nm emission comes from dissociative recombination process ($O_2^+ + e \rightarrow O + O^*(^1D)$), followed by radiative process ($O^*(^1D) \rightarrow O(^3P) + h\nu$ (λ = 630.0 nm)), whereas the OI 777.4 nm emission comes from radiative recombination process ($O^+ + e \rightarrow O^* + O^*$) followed by radiative process ($O^*(^5P) \rightarrow O^*(^5S) + h\nu$ (λ = 777.4 nm)). The simultaneous wide-angle imaging observations of the large-scale ionospheric plasma irregularities, seen through the OI 630.0 nm and OI 777.4 nm emissions, are unique optical observational technique that permits determination of the height resolved zonal plasma drifts. As pointed out by *Weber et al.* [1996], airglow images at 630.0 nm and 777.4 nm emissions provide information about the plasma density at two different altitudes because of the different airglow production mechanisms. The emission peak altitudes are separated by ~50–80 km in the *F* region [see, e.g., *Weber et al.*, 1982; *Mendillo et al.*, 1985]. It should be mentioned that the OI 777.4 nm emission (its intensity depends on the square of the peak electron density [*Tinsley and Bittencourt*, 1975]) comes from a wider layer centered near the *F* region peak (~300–380 km), whereas the OI 630.0 nm emission (its intensity is proportional to the product of the O^+ and O_2 concentrations) comes from a relatively narrow layer centered below the *F* region peak (~250–300 km) in region of increasing O_2 abundance.

[4] The early ionosphere-thermosphere studies based on the wide-angle imaging system observing the nightglow OI 630.0 nm emission line have been quite successful, in view of the fact that this emission line is very intense and the has a moderate dependence on solar activity [*Weber et al.*, 1978; *Mendillo and Baumgardner*, 1982; *Sahai et al.*, 1994, 2000]. It is important to mention that the $O(^1D)$ state is metastable and has a radiative lifetime of 110 s. Therefore the observed large-scale plasma depletions in wide-angle images, appearing as dark structures, are seen blurred or diffused because of the large radiative lifetime. However, with the recent advances in electro-optical technology and development of high-sensitivity cooled CCD cameras, the quality of the wide-angle imaging systems considerably improved and opened up new perspectives for ionosphere-thermosphere studies, including obtaining images with good signal/noise ratios for weak emissions, for example, the OI 777.4 nm emission, which is much weaker than the OI 630.0 nm emission and has high dependence on solar activity [*Mendillo et al.*, 1997; *Makela et al.*, 2001; *Abalde et al.*, 2001; *Otsuka et al.*, 2002]. Since at *F* region heights, the concentrations of O^+ and electrons are nearly equal, the emission rate is independent of the layer height but it is mainly dependent on the concentration near the *F* layer peak. This emission is prompt and consequently their images are not subject to the blurring effect.

[5] In this paper we present and discuss the nocturnal zonal plasma drift velocities obtained from the west to east motion of large-scale plasma depletion structures observed from simultaneous all-sky (field of view 180°) images in the two emissions for several days of 2000 and 2001. Recently, *Pimenta et al.* [2001] have presented an improved technique for the determination of the zonal plasma bubble drift velocities using the OI 630.0 nm emission all-sky images. In their technique, first the images are linearized using an appropriate geographic coordinate system. Then, the plasma intensity depleted regions, in consecutive image slices, using the bubble western wall, the minimum intensity depletion point, and the eastern wall, are compared to obtain the west-east plasma bubble drift velocities. They observed that the plasma bubbles shapes and dimensions change with space-time dynamics and discussed the observed different dynamic behavior related to the eastern and western walls and the minimum intensity depletion point of the plasma bubbles and inferred that the western walls are much more stable than the eastern wall and the minimum intensity depletion point. Therefore in the present paper we have used the motion of the bubble western walls to infer the zonal plasma drift velocities using both the emission images.

2. Observation and Instrumentation

[6] Simultaneous nighttime observations of the OI 630.0 nm and OI 777.4 nm emissions, using two multichannel all-sky imaging systems (for the observations reported in this paper, the two emissions were observed using two similar imaging systems) have been made at São José dos Campos (23.2°S, 45.9°W; dip latitude 17.6°S; hereafter referred as SJC), Brazil, a station under the equatorial ionospheric anomaly, during the years 2000 and 2001. The ionospheric sounding observations presented here, using a Canadian Advance Digital Ionosonde (CADI), are being carried out from the same location on a routine basis since July 2000. Figure 1 shows details of the all-sky imaging system coverage areas for the two emissions. It may be noted that the area covered by the OI 630.0 nm emission is slightly smaller than that covered by the OI 777.4 nm emission. In previous studies we assumed the emission heights for the OI 630.0 nm and OI 777.4 nm emissions as 300 and 380 km, respectively. In the present study we have used simultaneous clear-sky imaging observations obtained on five nights (three in spring equinox and two in summer; two nights are from the year 2000 and three from 2001) during quiet geomagnetic conditions and high solar activity, with the presence of large-scale ionospheric plasma depletions.

2.1. All-Sky Imaging System

[7] Two similar multispectral all-sky imaging system (Keo Consultants, Boston) have been used in the present investigations. The imaging systems use 4-inch diameter interference filters with 2.0 nm and 1.5 nm bandwidths for the OI 630.0 nm and OI 777.4 nm emissions, respectively. The CCD system used in the imaging systems (CH350 Photometrics detectors) consists of a large area of 6.45 cm^2, high resolution, and 1024 × 1024 back-illuminated array with a pixel depth of 14 bits. The high quantum efficiency (approximately 80% at visible wave-

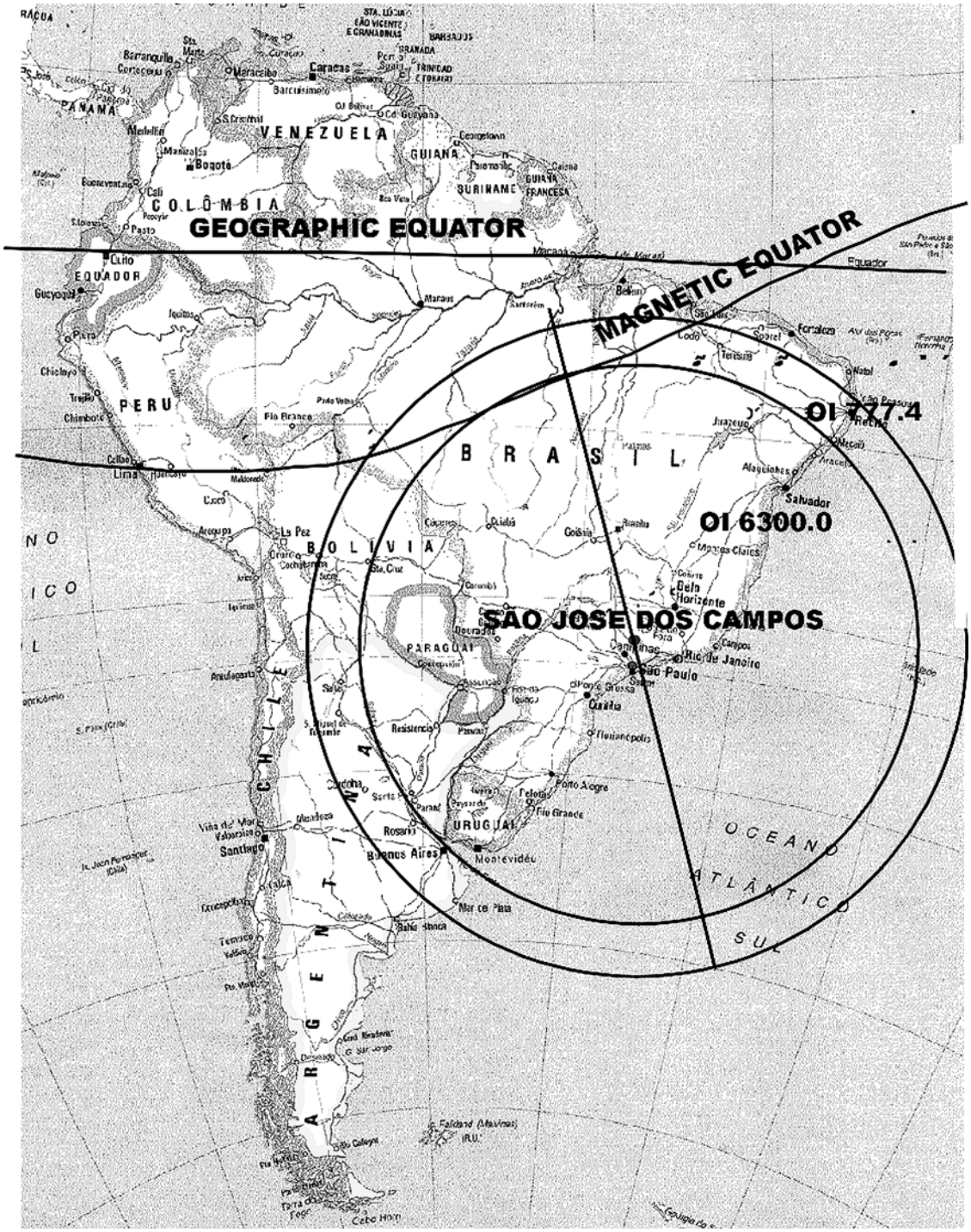

Figure 1. Coverage area for the OI 630.0 nm and OI 777.4 nm emissions, assuming emission peak altitudes at 300 km and 380 km, respectively, when the all-sky imaging system is located at Sao Jose dos Campos (23.2°S, 45.9°W). The local time is UT−3 hours.

lengths), low dark current (0.5 electrons/pixel/s), low readout noise, and high linearity (0.05%) of this device provide an excellent capability for quantitative measurements of the OI 630.0 nm and OI 777.4 nm nightglow emissions. The imaging system uses a fast (f/4) all-sky (180°) Mamiya 24 mm telecentric lens system, with a single interference filter and with binning on-chip down to a 512 × 512 image resolution. This configuration enables high signal-to-noise ratio images of the wave/plasma structures, with integration exposure time rates of 60 s for the OI 630.0 nm and 90 s for the OI 777.4 nm emissions. The images are recorded at intervals of 3 min.

2.2. Digital Ionosonde

[8] The Canadian Advanced Digital Ionosonde (CADI) operates from 1 to 20 MHz at vertical incidence and covers

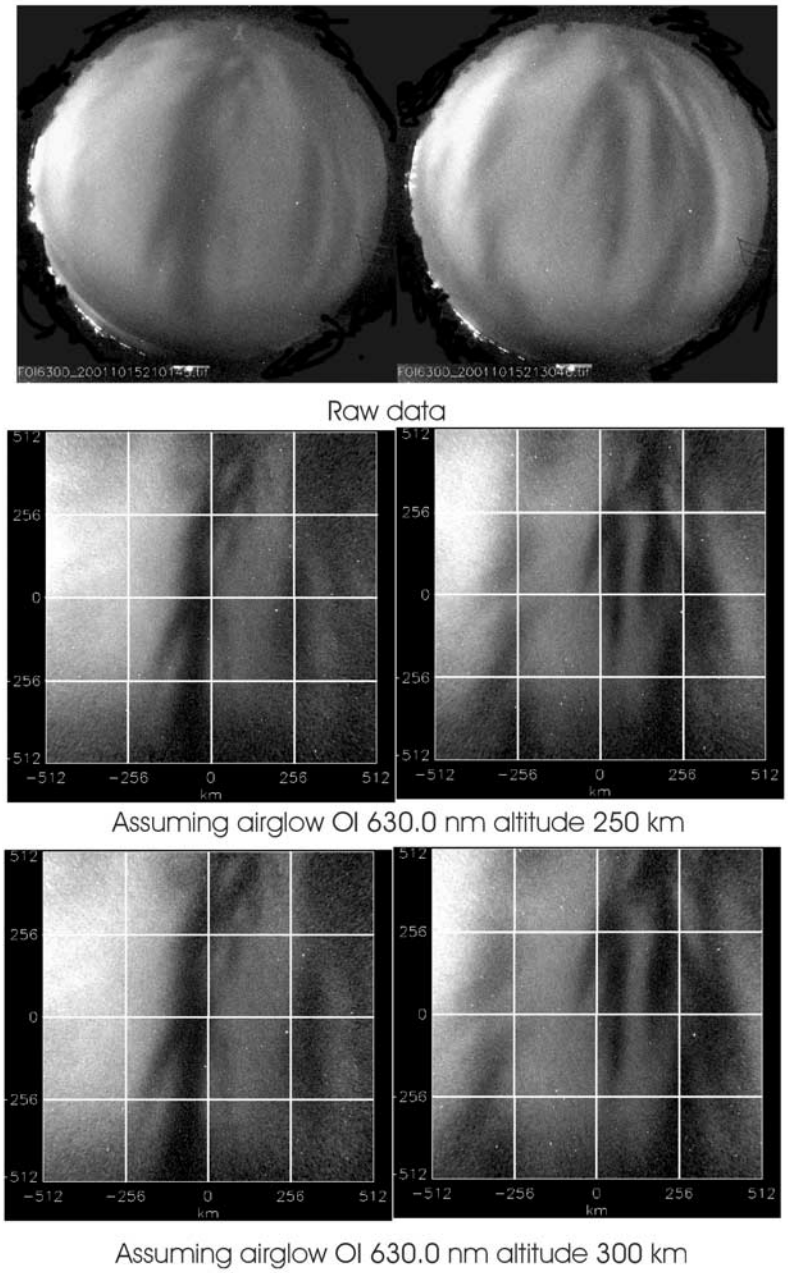

Figure 2. All-sky airglow images at OI 630.0 nm observed at São Jose dos Campos, Brazil, on 15 October 2001. The local times are 2101:45 (left) and 2130:46 (right). The images are raw (top) and linearized assuming emission peak altitudes of 250 km (middle) and 300 km (bottom). The linearized images are divided in 16 cells, with the top left cell being (1,1).

an altitude range between 90 km and 1000 km, approximately. The output pulses from the digital ionosonde, with power 600 W, have a length of 40 μs, giving a basic 6 km height resolution. When it operates in a Barker sequence of length 13, the output pulse is 13 × 40 μs and the 13 "chirps" are phase coded by ±90° in a special way. The advantage is that the effective output power will be 13 × 600 W = 7.8 kW.

[9] The Direct Digital Synthesis (DDS Card) produces the output waveforms of the local oscillator frequency and the RF frequency as a 10 bit digital number. These are converted to voltages by the two D/A converters. The DDS board also produces a 781 kHz reference frequency ("I" signal with 0° phase and "Q" signal with 90° phase). The transmitter provides power amplification of the RF signals. The receiver, which amplifies and demodulates the return signals, has a standard wideband RF amplifier, a mixer, and a narrowband IF amplifier at 781 kHz. The signal is then split and mixed with the "I" and "Q" 781 kHz reference signals (effectively mixing down to DC since the IF is reference frequency). The outputs from this mixing are DC voltages and these are sampled and digitized by the A/D converters. The digitized samples are correlated with the Barker sequence,

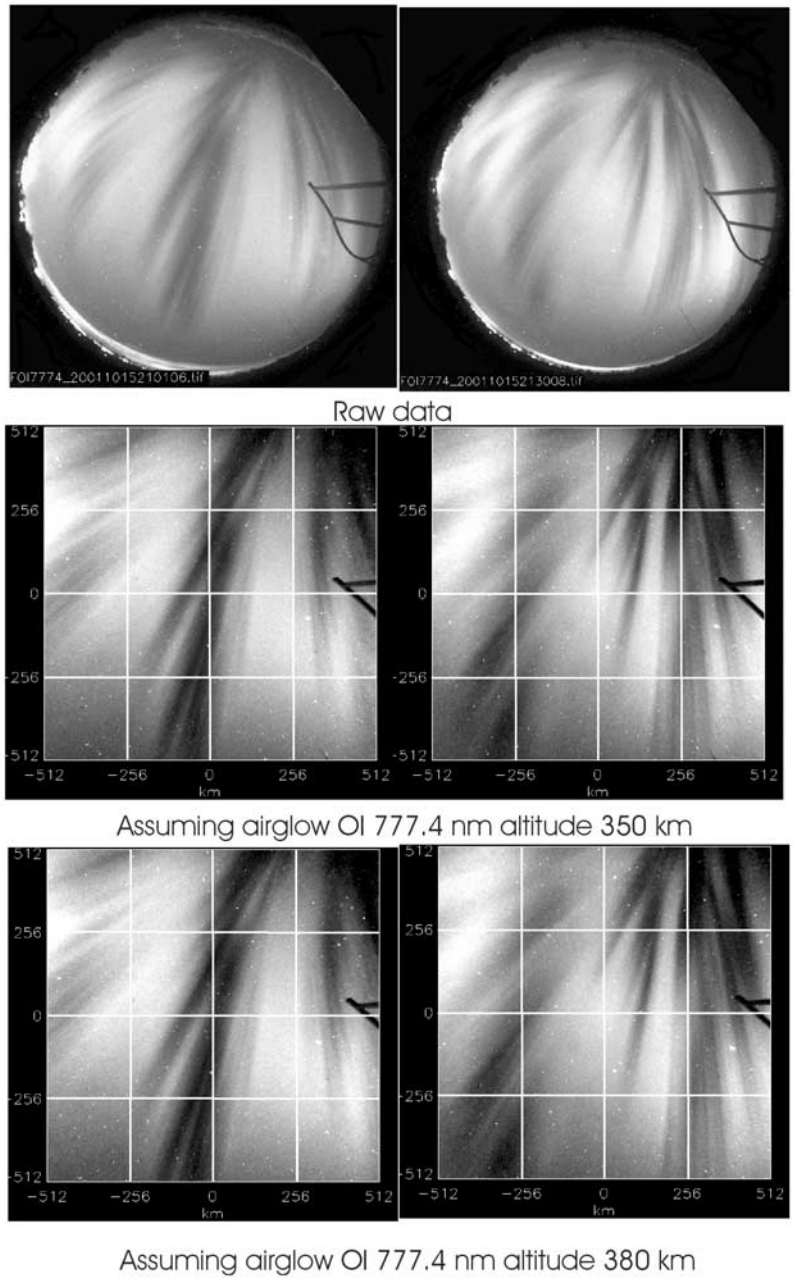

Figure 3. All-sky airglow images at OI 777.4 nm observed at São Jose dos Campos, Brazil, on 15 October 2001. The local times are 2101:06 (left) and 2130:08 (right). The images are raw (top) and linearized assuming emission peak altitudes of 350 km (middle) and 380 km (bottom).

if Barker coding is being used, and then downloaded to the computer.

[10] The received pulses may be coherently averaged to give an additional increase in the S/N ratio proportional to the number of pulses averaged. FFT processing may be used to remove the linear portion of the phase drift, when the ionosphere is sufficiently nonstationary; otherwise, phase coherence would be lost during averaging.

3. Data Analysis

[11] Figures 2 and 3 (top) show two examples of the OI 630.0 nm and OI 777.4 nm emissions images, respectively, observed ~30 min apart at SJC, on 15 October 2001, with the presence of large-scale quasi north-south magnetic field-aligned ionospheric plasma irregularities (dark structures). In spite of the fact that the two images shown in the top parts of Figures 2 and 3 are looking at the same part of the sky, with plasma depletions structures at almost the same time, the plasma structures appear different. The spatial irregularity structures seen though the OI 777.4 nm emission (Figure 3, top) show ray-like thin patterns, whereas the structures seen though the OI 630.0 nm (Figure 2, top) are diffused or blurred. The causes for this difference have been discussed in detail by *Abalde et al.* [2001].

[12] Also, it should be pointed out that the raw images are distorted, curved, and compressed at the edges (low elevation angles) and inflated in the center or zenith (high

elevation angles) due to the effect of the fish-eye lens. Therefore for any quantitative analysis, these images need to be first linearized to remove the effects of the fish-eye lens.

[13] In order to calculate the zonal (east-west) plasma drift velocities, as a function of local time, first we have to consider emission peak altitudes for both the emissions and transform the raw images into linear grid images, using the linearization method [*Garcia et al.*, 1997; *Pimenta et al.*, 2001, 2003]. The choice of these emission peak altitudes is important because the linearized images are slightly different when we assume different peak heights. The width and length of the dark structures, seen on the linearized images, are slightly modified, and these modifications affect the inferred zonal plasma drift velocities.

[14] The middle and bottom parts of Figures 2 and 3 show examples of the linearized images (1024 × 1024 km area), extracted from the circular fields shown in top part of Figures 2 and 3, assuming two different emission peak altitudes. The horizontal and vertical lines have been included to divide each linearized image into 16 cells to allow better visualization of the slight differences due to the assumption of different emission peak altitudes. The notation cell (x, y) to identify different cells is x = 1, 2, 3, and 4 from left to right and y = 1, 2, 3, and 4 from below to top (e.g., cell (4, 4) refers to the top right corner cell).

[15] Figure 2 presents two linearized OI 630.0 nm images, observed at 2101:45 LT (left) and 2130:46 LT (right), for two emission peak altitudes, 250 km (middle) and 300 km (bottom). Comparing some details in the middle and bottom left-hand images, cell (2, 2), it is noted that the dark structure in the middle is thinner than that seen in the bottom. Also, the dark structures in the bottom right-hand side, cells (3, 2) and (3, 3), are enlarged and displaced toward right, as compared with the middle right-hand side.

[16] Similarly, Figure 3 shows two linearized OI 777.4 nm images, observed at 2101:06 LT (left) and 2130:46 LT (right), for two emission peak altitudes, 350 km (middle) and 380 km (bottom). Comparing the middle and bottom left-hand images, cell (2, 3), it is noted that the dark structure in the middle is thinner than that seen in the bottom. Also, the dark structures in the bottom right-hand side, cell (4, 1), are thicker than the ones in the middle right-hand side.

[17] Since the present technique used to calculate the plasma drift velocities is based on space-time displacements of the western walls of dark structures (which are the optical signatures of large-scale plasma bubbles), we have used similar linearized images, as shown Figures 2 and 3, in the present investigation. Since the assumed emission peak altitude alters the widths and sizes of the dark structures, as discussed earlier, consequently changing the emission peak altitude is likely to influence the inferred plasma drift velocity, either being superestimated or underestimated. This may result in slight changes in the calculated nighttime zonal plasma drift velocities.

4. Results and Discussion

[18] Figure 4 shows the zonal plasma drift velocities inferred from all-sky image observations of the OI 630.0 nm and OI 777.4 nm emissions using linearized images assuming fixed emission peak altitudes of 300 km and 380 km, respectively, based on earlier investigations [*Mendillo and Baumgardner*, 1982; *Sobral and Abdu*, 1990, 1991; *Mendillo et al.*, 1997] and displacements of the western walls [*Pimenta et al.*, 2001, 2003] of the intensity depletion bands (dark structures, as shown in Figures 2 and 3) on five nights: 23–24 October 2000, 31 October to 1 November 2000, 21–22 February 2001, 15–16 October 2001, and 18–19 December 2001 (three in spring equinox and two in summer). The average maximum and minimum zonal drift velocities from the OI 630.0 nm emission are 185 ± 10 and 104 ± 18 m/s, whereas the average maximum and minimum zonal drift velocities from the OI 777.4 nm emission are 202 ± 19 and 121 ± 20 m/s.

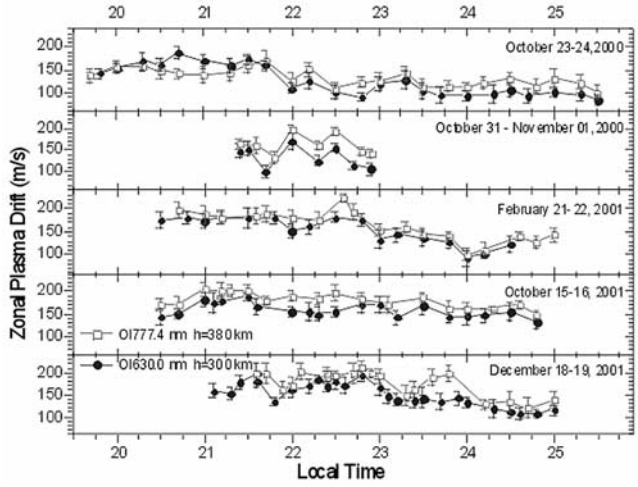

Figure 4. Zonal plasma drift velocities inferred from the OI 630.0 nm and OI 777.4 nm emissions all-sky observations using linearized images assuming emission peak altitudes of 300 km and 380 km, respectively, and displacements of the western walls of the intensity depletion bands (dark structures as shown in Figures 2 and 3).

[19] It is seen in Figure 4 that in general, the zonal plasma drift velocities obtained from the OI 777.4 nm emission are higher than those obtained from the OI 630.0 nm emission, but it is also noted that there are periods when the zonal plasma drift velocities obtained by one emission do not follow the local time variations obtained from the other emission. The latter result is surprising because it indicates that two close-by regions in the *F* layer are not showing similar local time variations. This could be possibly due to the assumption of fixed emission peak altitudes for the two emissions, since there may be considerable *F* region height changes during the course of a night. Therefore we recalculated the zonal plasma drift velocities from the two emissions using *F* region altitudes for the two emissions obtained from simultaneous ionospheric sounding observations carried out at the same location.

[20] Figure 5 shows the variations of the ionospheric *F* region sounding parameters, the minimum virtual height (h′*F* is the upper line) and virtual height at 0.834 of fo*F*2 (hp*F*2 is the lower line) (left-hand side), and the critical frequency (fo*F*2) variations (right-hand side), observed at São José dos Campos on five nights: 23–24 October 2000,

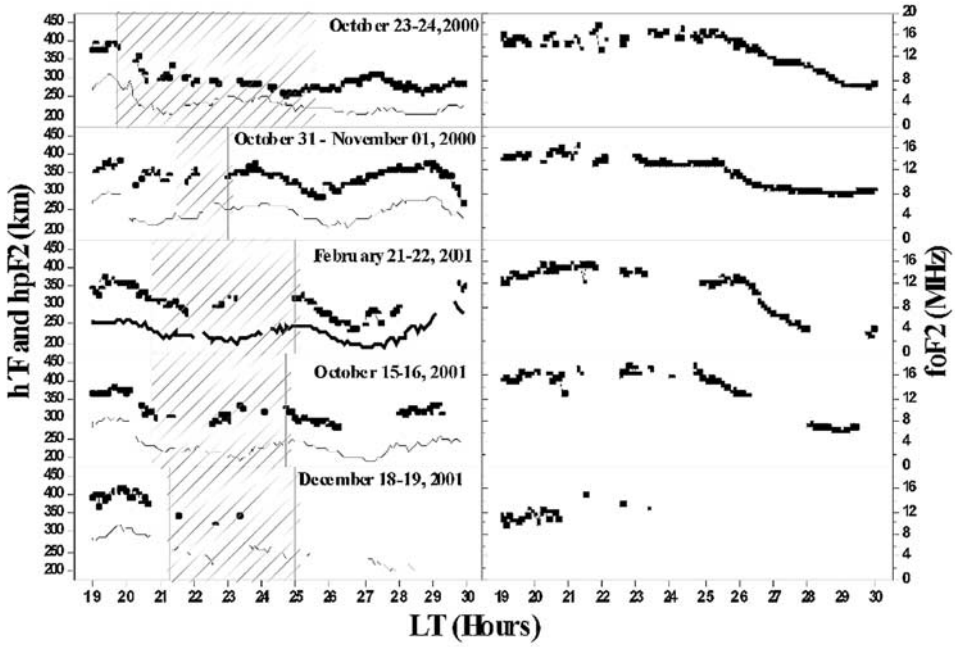

Figure 5. *F* region minimum virtual height (h′*F* is upper line) and virtual height at 0.834 of fo*F*2 (hp*F*2 is lower line) variations (left-hand side), and critical frequency (fo*F*2) variations (right-hand side), observed at low-latitude station São José dos Campos on five nights: 23–24 October 2000, 31 October to 1 November 2000, 21–22 February 2001, 15–16 October 2001, and 18–19 December 2001. The hatched portions indicate the period of imaging observations.

31 October to 1 November 2000, 21–22 February 2001, 15–16 October 2001, and 18–19 December 2001. As pointed out by *Danilov and Morozova* [1985], hp*F*2 is fairly close to the *F* region peak height during the nighttime. A perusal of the period of imaging observations on different nights in Figure 5 indicates that hp*F*2 shows height changes during the course of the optical measurements only on the night of 23–24 October. On the other nights, the hp*F*2 variations do not show much change during the periods of the optical observations. On the basis of these considerations, we have recalculated the zonal plasma drift velocities using the same technique described earlier but assuming the OI 777.4 nm emission peak height close to the average hp*F*2 values and the OI 630.0 nm emission peak height ~50–80 km below the average hp*F*2 (but not below h′*F*).

[21] Figure 6 shows the zonal plasma drift velocities recalculated for both the emissions and for the same five nights (Figure 5) but assuming different emission peak altitudes for four nights and three different values in the case of the night 23–24 October 2000, as follows: post-sunset (1930 to 2030 LT; emission peak altitudes assumed of 300 km and 350 km for the OI 630.0 nm and OI 777.4 nm emissions, respectively); early night (2045 to 2230 LT; emission peak altitudes assumed of 250 km and 300 km for the OI 630.0 nm and OI 777.4 nm emissions, respectively), and midnight (2245 to 0130 LT; emission peak altitudes assumed of 270 km and 310 km for the OI 630.0 nm and OI 777.4 nm emissions, respectively). For the other four nights, the emission peak altitudes assumed were as follows: 31 October to 1 November 2000, 300 km and 350 km for the OI 630.0 nm and OI 777.4 nm emissions, respectively; 21–22 February 2001 and 15–16 October 2001, 280 km and 330 km for the OI 630.0 nm and OI 777.4 nm emissions, respectively; and 18–19 December 2001, 280 km and 350 km for the OI 630.0 nm and OI 777.4 nm emissions, respectively. The average maximum and minimum zonal drift velocities from the OI 630.0 nm emission are 172 ± 2 and 89 ± 15 m/s, respectively, whereas the average maximum and minimum zonal drift velocities from the OI 777.4 nm emission are 184 ± 12 and 103 ± 16 m/s,

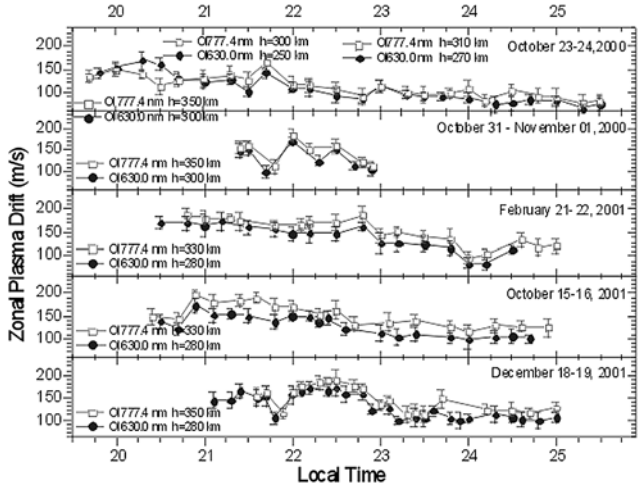

Figure 6. Zonal plasma drift velocities recalculated for the OI 630.0 nm and OI 777.4 nm emissions using the displacements of the western walls of the intensity depletions (dark structures of Figures 2 and 3) for linearized images assuming different emission peak altitudes based on the simultaneous ionospheric sounding observations.

Table 1. Calculated Average Zonal Plasma Drift Velocities

Date	Season	Zonal Plasma Drift Velocities Assuming Emission Peak Altitudes Based on Earlier Investigations				Zonal Plasma Drift Velocities Assuming Emission Peak Altitudes Based on Simultaneous Ionospheric *F* Region Parameters			
		OI 630.0 nm m/s		OI 777.4 nm m/s		OI 630.0 nm m/s		OI 777.4 nm m/s	
		Minimum	Maximum	Minimum	Maximum	Minimum	Maximum	Minimum	Maximum
23–24 Oct 2000	Equinox	85	188	102	173	65	170	78	165
31 Oct to 1 Nov 2000	Equinox	101	170	134	199	101	170	113	184
15–16 Oct 2001	Equinox	132	188	147	204	98	173	115	196
21–22 Feb 2001	Summer	94	181	100	224	83	175	97	188
18–19 Dec 2001	Summer	108	198	120	212	98	172	112	188
Average Values		104 ± 18	185 ± 10	121 ± 20	202 ± 19	89 ± 15	172 ± 2	103 ± 16	184 ± 12

respectively. The average maximum and minimum zonal plasma drift velocities for both the emissions in the present calculations are lower and with less scatter than those presented earlier using fixed assumed emission peak altitudes. Also, the nocturnal variations of the zonal plasma drift velocities obtained for the two emissions with peak altitudes based on simultaneous ionospheric observations show better agreement than for the case with fixed emission peak altitudes (h = 380 km for OI 777.4 nm and h = 300 km for OI 630.0 nm). For the five nights studied in the present investigations, the average correlation coefficient (r), with fixed emission peak altitudes $r = 0.89$, whereas with emission peak altitudes based on the simultaneous ionospheric observations $r = 0.93$.

[22] Table 1 shows the average zonal plasma drift velocities calculated for the two different cases investigated in this work. It is noted from Table 1 that both the calculations show that the zonal plasma drift velocities are slightly higher in the case of the OI 777.4 nm emission than that for the OI 630.0 nm emission. It should be pointed out that the uncertainties in the average values (maximum and minimum drifts in Table 1) reported are associated with both the variability in geophysical conditions and errors in the drift velocity determination method used. Also, the zonal plasma drift velocities have similar values in both the equinox and summer seasons.

[23] The observed OI 630.0 nm emission zonal plasma drift velocities in low-latitude region are comparable with those reported by *Sobral and Abdu* [1990, 1991, 1999] but slightly higher than those presented by *Mendillo and Baumgardner* [1982], *Taylor et al.* [1997], *Santana et al.* [2001], *Otsuka et al.* [2002], and *Pimenta et al.* [2003]. This is possibly because the emission peak altitude assumed in the present case is higher. *Pimenta et al.* [2003] have reported that "if the OI 630.0 nm emission peak altitude is considered as 300 km, instead of 250 km, the plasma drift velocities increase by about 20%", i.e., the plasma drift velocities increase by ~20% for 50 km height increase in the assumed emission peak altitude. Also, this difference could be attributed, in some cases, to the different magnetic latitudes of the observing sites. Recent results have shown that plasma, in the vicinity of the equatorial ionospheric anomaly, can have a larger eastward speed than would be expected if one referred to the vicinity of equatorial region [*Kil et al.*, 2000; *Immel et al.*, 2003; *Martinis et al.*, 2003].

[24] The observed nocturnal variations of the zonal plasma drift velocities inferred from the OI 630.0 nm emission, that is, decrease from evening hours to midnight, are similar to those reported by *Woodman* [1972], *Malcolm et al.* [1984], *Fejer et al.* [1985], *Sobral and Abdu* [1991, 1999], *Taylor et al.* [1997], *Otsuka et al.* [2002], and *Pimenta et al.* [2003]. Also, the observed nocturnal variations are fairly similar to the zonal neutral wind velocities reported by *Sahai et al.* [1992] from the low-latitude region in Brazil, for these seasons.

[25] The observed OI 777.4 nm emission zonal plasma drift velocities are fairly similar in behavior but slightly higher than the OI 630.0 nm drift velocities. This fact indicates that the zonal plasma drifts near the peak of the F layer are slightly higher than at the bottomside of the F

layer. The observed simultaneous OI 630.0 nm and OI 777.4 nm emissions zonal plasma drifts are much higher than those reported by *Mendillo et al.* [1997] from similar observations at Arequipa, Peru.

5. Conclusions

[26] Simultaneous observations in the OI 630.0 nm and OI 777.4 nm emission all-sky imaging observations carried out from a low-latitude station in Brazil have been used to infer the nighttime zonal plasma drift velocities. Since the two emissions originate from the *F* region bottomside (OI 630.0 nm) and peak height (OI 777.4 nm), it was possible to calculate the nighttime zonal plasma drift variations at two different *F* layer heights. In this paper we have investigated the nighttime zonal plasma drift variations using fixed emission peak altitudes, used by earlier investigators, as well as emission peak altitudes based on simultaneous ionospheric sounding observations. The main results are presented below.

[27] 1. For the case of fixed emission peak altitudes, the average maximum and minimum zonal drift velocities, inferred from the OI 630.0 nm emission, are 185 ± 10 and 104 ± 18 m/s, whereas the average maximum and minimum zonal drift velocities from the OI 777.4 nm emission are 202 ± 19 and 121 ± 20 m/s.

[28] 2. For the case of emission peak altitudes based on simultaneous ionospheric observations, the average maximum and minimum zonal drift velocities, inferred from the OI 630.0 nm emission, are 172 ± 2 and 89 ± 15 m/s, whereas the average maximum and minimum zonal drift velocities from the OI 777.4 nm emission are 184 ± 12 and 103 ± 16 m/s.

[29] 3. The average maximum and minimum zonal plasma drift velocities inferred for both the emissions, using emission peak altitudes based on simultaneous ionospheric observations, are lower and with less scatter than those using fixed emission peak altitudes. Also, the nocturnal variations with emission peak altitudes based on simultaneous ionospheric observations show better agreement between the zonal plasma drift velocities obtained from the two emissions than for the case with fixed emission peak altitudes.

[30] 4. During the course of a night, in general, the zonal plasma drift velocities inferred from the OI 777.4 nm emission are slightly higher than those inferred from the OI 630.0 nm emission, indicating that the plasma drift velocities near the *F* layer peak height are slightly higher than that at the bottomside of the *F* layer. Also, in both emissions the zonal plasma drift velocities decrease from evening hours to midnight.

[31] 5. Simultaneous optical and ionosonde observations are becoming increasingly important for a better understand of ionosphere dynamics and thermosphere-ionosphere coupling.

[32] **Acknowledgments.** The authors acknowledge the Fundação de Amparo à Pesquisa do Estado de São Paulo (FAPESP) through processes 1998/09892-0 and 2002/06131-5 and the Conselho Nacional de Desenvolvimento Científico e Tecnológico (CNPq) through processes 301222/2003/7, 300843/2003-8, and 305625/2003-9 for the support received.

[33] Arthur Richmond thanks Thomas Immel and Brian Tinsley for their assistance in evaluating this paper.

References

Abalde, J. R., P. R. Fagundes, J. A. Bittencourt, and Y. Sahai (2001), Observations of equatorial F region plasma bubbles using simultaneous OI 777.4 nm and OI 630.0 nm imaging: New results, *J. Geophys. Res.*, *106*(A12), 30,331–30,336.

Abdu, M. A., J. H. Sobral, Y. Nakamura, and C. J. Zamlutti (1987), Equatorial plasma bubble zonal velocity height gradient from spaced VHF polarimeter and scanning 630 nm measurements, *Geophys. Res. Lett.*, *14*(9), 965–968.

Aggson, L. T., N. C. Maynard, F. A. Herrero, H. G. Mayr, L. H. Brace, and M. C. Liebrecht (1987), Geomagnetic equatorial anomaly in zonal plasma flow, *J. Geophys. Res.*, *92*(A1), 311–315.

Basu, Sa., Su. Basu, E. Kudeki, H. P. Zengingonul, M. A. Biondi, and J. W. Meriwether (1991), Zonal irregularity drifts and neutral winds measured near the magnetic equator in Peru, *J. Atmos. Terr. Phys.*, *53*(8), 743–755.

Basu, Su., et al. (1996), Scintillations, plasma drifts, and neutral winds in the equatorial ionosphere after sunset, *J. Geophys. Res.*, *101*(A12), 26,795–26,809.

Bhattacharyya, A., S. J. Franke, and K. C. Yeh (1989), Characteristic velocity of equatorial F region irregularities determined from spaced receiver scintillation data, *J. Geophys. Res.*, *94*(A9), 11,959–11,969.

Biondi, M. A., J. W. Meriwether Jr., B. Fejer, and R. Woodman (1988), Measurements of the dynamics and coupling of the equatorial thermosphere and F-region ionosphere in Peru, *J. Atmos. Terr. Phys.*, *50*(10/11), 937–942.

Coley, W. R., and R. A. Heelis (1989), Low-latitude zonal and vertical ion drifts seen by DE 2, *J. Geophys. Res.*, *94*(A6), 6751–6761.

Danilov, A. D., and L. D. Morozova (1985), Ionospheric storms in the F2 region. Morphology and physics (Review), *Geomagn. Aeron.*, *25*(5), 593–605.

dePaula, et al. (2002), Ionospheric irregularity zonal velocities over Cachoeira Paulista, *J. Atmos. Terr. Phys.*, *64*(12), 1511–1516.

Fagundes, P. R., Y. Sahai, I. S. Batista, J. A. Bittencourt, M. A. Abdu, and H. Takahashi (1997), Vertical and zonal equatorial F-region plasma bubble velocities determined from OI 630 nm nightglow imaging, *Adv. Space Res.*, *20*(6), 1297–1300.

Fejer, B. G., E. Kudeki, and D. T. Farley (1985), Equatorial *F* region zonal plasma drifts, *J. Geophys. Res.*, *90*(A12), 12,249–12,255.

Garcia, F. J., M. J. Taylor, and M. C. Kelley (1997), Two-dimensional spectral analysis of mesospheric airglow image data, *Appl. Opt.*, *36*(29), 7374–7385.

Immel, T. J., S. B. Mende, H. U. Frey, and L. M. Peticolas (2003), Determination of low latitude plasma drift speeds from FUV images, *Geophys. Res. Lett.*, *30*(18), 1945, doi:10.1029/2003GL017573.

Kil, H., P. M. Kintner, E. R. dePaula, and I. J. Kantor (2000), Global Positioning System measurements of the ionospheric zonal apparent velocity at Cachoeira Paulista in Brazil, *J. Geophys. Res.*, *105*(A3), 5317–5327.

Makela, J. J., M. C. Kelley, S. A. González, N. Aponte, and R. P. McCoy (2001), Ionospheric topography maps using multiple-wavelength all-sky images, *J. Geophys. Res.*, *106*(A12), 29,161–29,174.

Malcolm, R., C. Miles, and B. A. Tinsley (1984), Field-aligned observation of trans-equatorial bubbles from Rarotonga in 1969–70, *Geophys. Res. Lett.*, *11*, 665–668.

Martinis, C., J. V. Eccles, J. Baumgardner, J. Manzano, and M. Mendillo (2003), Latitude dependence of zonal plasma drifts obtained from dual-site airglow observations, *J. Geophys. Res.*, *108*(A3), 1129, doi:10.1029/2002JA009462.

Mendillo, M., and J. Baumgardner (1982), Airglow characteristics of equatorial plasma depletions, *J. Geophys. Res.*, *87*, 7641–7652.

Mendillo, M., H. Spence, and S. T. Zalesak (1985), Simulation studies of ionospheric airglow signatures of plasma depletions at equator, *J. Atmos. Terr. Phys.*, *47*, 885–893.

Mendillo, M., J. Baumgardner, M. Colerico, and D. Nottingham (1997), Imaging science contributions to equatorial aeronomy: Initial results from the MISETA program, *J. Atmos. Terr. Phys.*, *59*(13), 1587–1599.

Otsuka, Y., K. Shiokawa, and T. Ogawa (2002), Geomagnetic conjugate observations of equatorial airglow depletions, *Geophy. Res. Lett.*, *29*(15), 1753, doi:10.1029/2002GL015347.

Pimenta, A. A., P. R. Fagundes, J. A. Bittencourt, Y. Sahai, D. Gobbi, A. F. Medeiros, M. J. Taylor, and H. Takahashi (2001), Ionospheric plasma bubble zonal drift: a methodology using OI 630 nm all-sky imaging systems, *Adv. Space Res.*, *27*(6/7), 1219–1224.

Pimenta, A. A., P. R. Fagundes, Y. Sahai, J. A. Bittencourt, and J. R. Abalde (2003), Equatorial F-region plasma depletion drifts: Latitudinal and seasonal variations, *Ann. Geophys.*, *21*, 2315–2322.

Sahai, Y., H. Takahashi, P. R. Fagundes, B. R. Clemesha, N. R. Teixeira, and J. A. Bittencourt (1992), Observations of thermospheric neutral winds at 23°S, *Planet. Space Sci.*, *40*(6), 767–773.

Sahai, Y., J. Aarons, M. Mendillo, J. Baumgardner, J. A. Bittencourt, and H. Takahashi (1994), OI 630 nm imaging observations of the equatorial plasma depletions at 16°S dip latitude, *J. Atmos. Terr. Phys.*, *56*, 1461–1475.

Sahai, Y., P. R. Fagundes, and J. A. Bittencourt (2000), Transequatorial F-region ionospheric plasma bubbles: Solar cycle effects, *J. Atmos. Terr. Phys.*, *62*, 1377–1383.

Santana, D. C., J. H. A. Sobral, H. Takahashi, and M. J. Taylor (2001), Optical studies of the ionospheric irregularities over the Brazilian region by nocturnal images of the OI 630 nm emission, *Adv. Space Res.*, *27*(6/7), 1207–1212.

Sobral, J. H. A., and M. A. Abdu (1990), Latitudinal gradient in the plasma bubble zonal velocities as observed by scanning 630-nm airglow measurements, *J. Geophys. Res.*, *95*(A6), 8253–8257.

Sobral, J. H. A., and M. A. Abdu (1991), Solar activity effects on equatorial plasma bubble zonal velocity and its latitude gradient as measured by airglow scanning photometers, *J. Atmos. Terr. Phys.*, *53*(8), 729–742.

Sobral, J. H. A., M. A. Abdu, H. Takahashi, H. Sawant, C. J. Zamlutti, and G. L. Borda (1999), Solar geomagnetic activity effects on nocturnal zonal velocities of ionospheric plasma depletions, *Adv. Space Res.*, *24*(11), 1507–1510.

Taylor, M. J., J.-M. Jahn, S. Fukao, and A. Saito (1997), Possible evidence of gravity wave coupling into the midlatitude *F* region ionosphere during the SEEK campaign, *J. Geophys. Res.*, *24*(13), 1699–1702.

Tinsley, B. A., and J. A. Bittencourt (1975), Determination of *F* region height and peak electron density at night using airglow emissions from atomic oxygen, *J. Geophys. Res.*, *80*(16), 2333–2337.

Tinsley, B. A., R. P. Rohrbaugh, W. B. Hanson, and A. L. Broadfoot (1997), Images of transequatorial *F* region bubbles in 630- and 777-nm emissions compared with satellite measurements, *J. Geophys. Res.*, *102*(A2), 2057–2077.

Valladares, C. E., J. W. Meriwether, R. Sheehan, and M. A. Biondi (2002), Correlative study of neutral winds and scintillation drifts measured near the magnetic equator, *J. Geophys. Res.*, *107*(A7), 1112, doi:10.1029/2001JA000042.

Weber, E. J., J. Buchau, R. Eather, and S. B. Mende (1978), North-south aligned equatorial airglow depletions, *J. Geophys. Res.*, *83*, 712–716.

Weber, E. J., H. C. Brinton, J. Buchau, and J. G. Moore (1982), Coordinated airborne and satellite measurements of equatorial plasma depletions, *J. Geophys. Res.*, *87*, 10,503–10,513.

Weber, E. J., et al. (1996), Equatorial plasma depletion precursor signatures and onset observed at 11° south of the magnetic equator, *J. Geophys. Res.*, *101*, 26,829–26,838.

Woodman, R. F. (1972), East-west ionospheric drifts at the magnetic equator, *Space Res.*, *XII*, 969–974.

J. R. Abalde, P. R. Fagundes, V. G. Pillat, and Y. Sahai, Universidade do Vale do Paraíba (UNIVAP), Av. Shishima Hifumi 2911, Urbanova, CEP 12224-000, São José dos Campos, São Paulo, Brazil. (abalde@univap.br; fagundes@univap.br; valdirgp@univap.br)

J. A. Bittencourt and A. A. Pimenta, Instituto Nacional de Pesquisas Espaciais (INPE), Cx. Postal 515, CEP 12201-970, São José dos Campos, São Paulo, Brazil. (pimenta@laser.inpe.br; bittenc@dae.inpe.br)